Click Here for Full Article

Robust Sahel drying in response to late 20th century forcings

Michela Biasutti[1] and Alessandra Giannini[2]

[1]   The African Sahel experienced severe drying between the 1950s and the 1980s, with partial recovery since. We compare Sahel rainfall in the 20th century, pre-industrial, and increased greenhouse gases (GHG) simulations produced for the Intergovernmental Panel on Climate Change (IPCC). The simulations forced by 20th century concentrations of aerosol and GHG reproduce (i) a global change in SST akin to that associated with Sahel drought and (ii) a correspondent drying of the Sahel. We conclude that late 20th century Sahel climate was significantly dryer than pre-industrial, and at least 30% of the drying was externally forced. Comparison between 20th century runs and runs forced by GHG alone reveals the key role of reflective aerosols: they force a gradient in SST that excites robust drying in the northern edge of the Atlantic Inter-Tropical Convergence Zone (ITCZ) and in the Sahel. **Citation:** Biasutti, M., and A. Giannini (2006), Robust Sahel drying in response to late 20th century forcings, *Geophys. Res. Lett.*, *33*, L11706, doi:10.1029/2006GL026067.

1.   Introduction

[2]   The semi-arid African Sahel, the southern edge of the Sahara, experienced severe drying between the 1950s and the 1980s, with partial recovery since [*Nicholson*, 1980; *Nicholson et al.*, 2000]. Recent studies showed that the long-term drying must be attributed to global sea-surface temperatures (SST), rather than anthropogenic land-surface modification: general circulation models (GCMs) of the atmosphere forced with the historic time series of SST reproduce, albeit often with reduced amplitude [*Giannini et al.*, 2003; *Zeng et al.*, 1999], the time series of Sahel rainfall [*Folland et al.*, 1986; *Giannini et al.*, 2003; *Tippett and Giannini*, 2006; *Lu and Delworth*, 2005; *Hoerling et al.*, 2006]. The concern for human influence on Sahel climate has thus shifted from local land-use practices [*Herrmann and Hutchinson*, 2005] to the effects of anthropogenic emissions on global SST.

[3]   Our data set is extracted from the simulations assembled for the fourth assessment report of the IPCC (a table characterizing the models is available via Web browser or via Anonymous FTP from ftp://ftp.agu.org/apend/; more information on the data set is at http://www-pcmdi.llnl.gov/). To compare externally forced and internal variability we analyze 20th-century (hereafter XX) and pre-industrial control integrations (hereafter PI) of 19 coupled models. Additionally, we consider two kinds of integrations in which GHGs are the dominant forcing: 12 idealized integrations forced solely by CO_2 concentration growing by 1% per year from pre-industrial levels and stabilizing at quadrupled the initial value (hereafter 4x), and 19 so-called A1B climate-change scenario integrations (hereafter A1B) in which CO_2 increases to 700 ppm over the 2000–2100 period, sulfate aerosols decrease, and natural forcings remain fixed.

[4]   We aim to determine whether mean rainfall in the Sahel (delimited herein as the 10N–20N zonal band across Africa) is significantly different in the XX and PI simulations. In XX, variability is forced by both anthropogenic (e.g., growing GHG and aerosols from industrialization) and, for about half the models, natural (solar variability and volcanic aerosols) forcings. In PI, all external forcings are fixed in time and variability is the pure expression of dynamics internal to the climate system. The weakness of this approach is that we cannot directly contrast model output to observations, due to a lack of instrumental records of Sahel rainfall during pre-industrial times. Its strength is that it can detect—to the extent that external forcings are accurately represented—the externally forced component of drought, independently of whether the sharp decline in Sahel rainfall from the 1950s to the mid 1980s was in part due to internal variability.

2.   Response to 20th Century Forcings

[5]   Figure 1 shows the difference between late 20th century and pre-industrial climate, hereafter the XX-PI difference. Figures 1a and 1b show the average XX-PI difference in annual mean surface temperature and June-July-August (JJA, the rainy season in the Sahel) rainfall; Figures 1c and 1d show a measure of model agreement (see caption for details). The XX-PI SST difference is characterized by warmer tropics, especially south of the equator, and cooler mid-latitudes, especially in the North Atlantic. This pattern strongly resembles both that associated with the historical Sahel drought [e.g., *Giannini et al.*, 2003] and the observed 1950–1999 trend [*Hansen et al.*, 1999]. The XX-PI JJA rainfall difference shows marked drying at the northern edge of the ITCZ, across the East Pacific, Atlantic, and Sahel, as well as in the monsoon regions of Asia, but increased rain in the west and south Pacific, and in the Gulf of Guinea. The cross-model consensus in reproducing a relatively small-scale feature such as the drying of the Sahel is truly remarkable, given large differences in model formulation and forcings, and the notorious difficulties of GCMs in simulating tropical rainfall.

[6]   A negative Sahel rainfall anomaly is a robust feature across models; how significant is it against the internal variability of each model? Figure 2a shows the XX-PI difference in JJA Sahel rainfall against the internal variability in 25-year mean rainfall, shown by the one and two

[1]Lamont-Doherty Earth Observatory, Columbia University, New York, USA.
[2]International Research Institute for Climate and Society, Columbia University, Palisades, New York, USA.
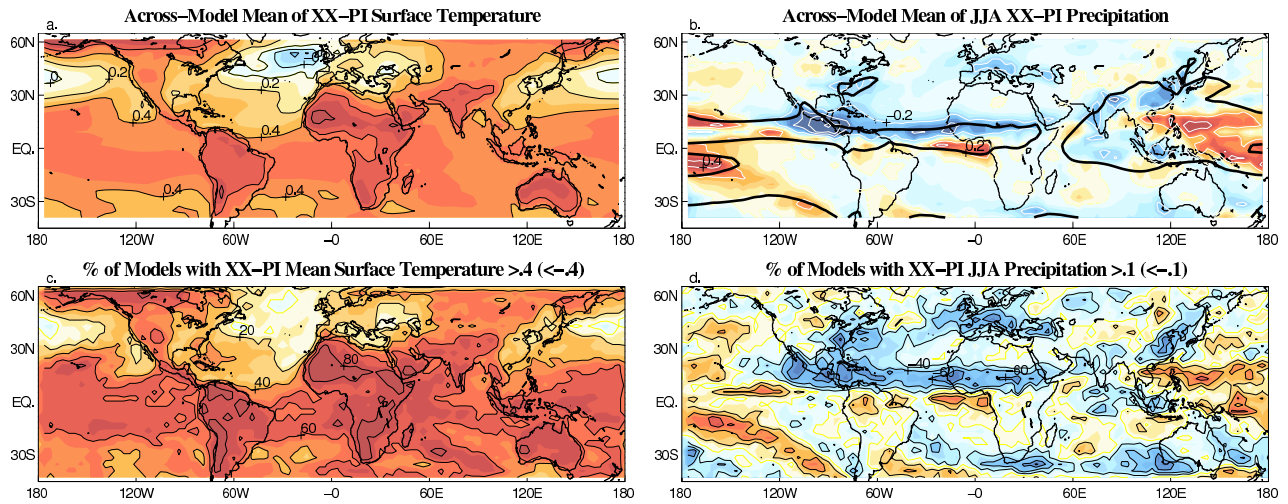
Figure 1. Difference between 1975–1999 mean climate in the XX simulations and pre-industrial (PI) climate. (a and c) Annual mean surface temperature. (b and d) JJA rainfall. Warm colors and solid contours indicate positive anomalies and cool colors and dashed contours indicate negative anomalies. Figures 1a and 1b show cross-model means (contour interval is 0.1C for temperature and 0.1 mm day 1 for rainfall), the thick black line in Figure 1b is the 4 mm day-1 contour in the XX simulations. Figures 1c and 1d a measure of inter-model agreement. A value of 1 (1) was assigned to models with XX-PI difference positive (negative) and larger than a threshold (0.4C or 0.1 mm day-1); the sum over all models is shown as percentages (c.i. 20%).
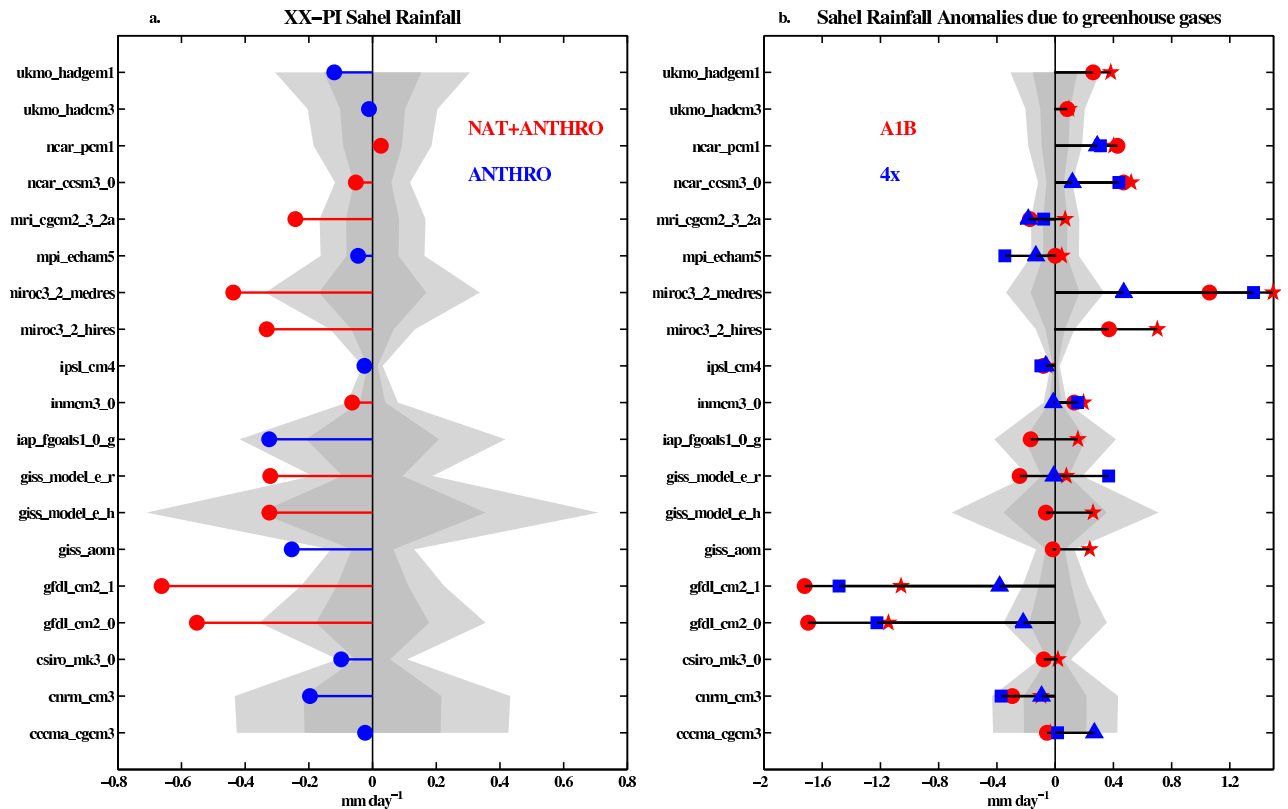

Figure 2. (a) The JJA Sahel rainfall difference between XX (1975–1999 ensemble mean for each model, circles and squares) and PI (long-term mean). The dark (light) gray shading are one (two) sigma deviations in 25-year mean Sahel rainfall in each PI simulation. Models forced by both natural and anthropogenic forcings shown in red circles, those forced only by anthropogenic forcings in blue squares. Note that the "red circle" models also tend to have a more complete treatment of aerosol forcings and to include land-use changes (see Table S1). Except for CCMA, PCM1 and HADCM3, drying is significant at the 95% level. (b) 25-year mean JJA Sahel rainfall anomalies: 4x-PI anomalies at two stages in the 4x runs [at late 20th century (triangles, yrs 50–75) and four times pre-industrial CO_2 concentration (squares, yrs 115–140)] and anomalies between the A1B runs (at CO_2 concentration of 700 ppm, yrs 75–100) and either the PI control (circles, A1B-PI) or the end of the XX simulations (stars, A1B-XX). Gray shading as in Figure 2a.
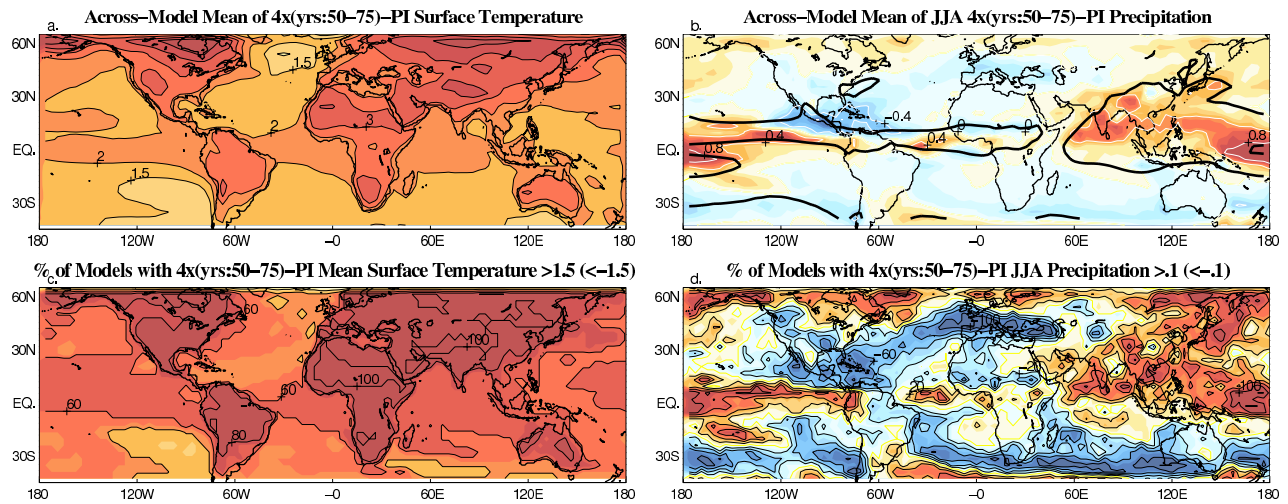
Figure 3. As for Figure 1, but for the 4x(yrs 50−75)-PI difference (12 models). (a and b) The contour interval is 0.2°C for temperature and 0.2 mm day^{-1} for rainfall. (c) The threshold is 1.5°C.

standard deviation limits estimated from the PI integrations. The XX-PI difference is significantly negative in a majority of models (16); in no case it is significantly positive. Such strong cross-model agreement forcefully suggests that observed dryness in the Sahel has been—at least in part—a response to late 20th century forcings.

[7] The above analysis establishes that the late 20th century Sahel drought had a forced component. Unfortunately, different modeling groups used different forcings for the XX integrations, including natural and anthropogenic, making attribution of drought to anthropogenic causes more complex. The forcings common across all XX simulations are anthropogenic: (i) the well-mixed GHGs and (ii) the direct effect of sulfate aerosols. Historic variations in solar and volcanic forcings, land use, carbonaceous aerosols, and ozone force about half of the simulations, and treatment of the semi-direct and indirect aerosols effects varies widely (Table S1 in auxiliary material[1]). We repeated our analysis on those models forced exclusively by anthropogenic emissions; they reproduce the large scale patterns of both SST and rainfall anomalies (see Figure 2a above and Figure S1 in auxiliary material). Moreover, the SST anomalies shown in Figure 1a have been linked to anthropogenic, not natural forcings [Cubasch et al., 2001] and [Rotstayn and Lohmann, 2002] have shown that aerosols force a hemispheric SST gradient and Sahel drought. Finally, simulations with the GFDL model confirm that natural forcings do not cause drying in the Sahel [Held et al., 2005]. Therefore, we shall focus on the effect of GHGs and reflective aerosols.

3. Response to Greenhouse Gases

[8] The SST anomalies responsible for Sahel dryness (Figure 1a) have been characterized as both an inter-hemispheric, or north/south gradient and a tropical warming. The different interpretations suggest different origins for the SST anomalies and different mechanisms for SST influence over the Sahel.

[9] GHG alone can force tropical warming and may slow down the ocean meridional overturning circulation (MOC), thereby reducing heat transport in the north tropical Atlantic and forcing a local north/south temperature gradient [Rahmstorf, 2002]. A combination of aerosols and GHG can induce a north/south gradient in SST warming because larger aerosol loadings in the Northern Hemisphere locally reduce the GHG-induced warming, via direct and indirect effects [Hansen et al., 2002].

[10] To understand the role of each forcing, we analyze the 4x simulations, in which only CO_2 varies. Figure 3 shows the 4x-PI difference in annual surface temperature and JJA rainfall when CO_2 concentration reaches late 20th century levels in the 4x integration. SST warming is maximum in the equatorial regions and weaker in the subtropics; the warming is especially symmetric about the equator in the Atlantic sector. Contrary to the XX-PI case, the 4x-PI difference shows no coherent drying of either the northern edge of the Atlantic ITCZ or the Sahel: the mean drying comes from only a fraction of the models (Figure 3d and 2b). The disagreement on the response of African rainfall to GHG forcing is best shown in Figure 2b. When the GHG forcing is the only (4x-PI) or dominant (A1B-PI and A1B-XX) forcing, models predict a dry Sahel about as often as a wet one. Thus, while models agree in ascribing the 20th century Sahel drought—at least partially—to anthropogenic emissions, they disagree in their prediction for a future, higher-GHG world [Held et al., 2005]. We propose that the robust XX-PI anomalies are due to the effect of aerosols, which induce a robust north/south SST gradient in the tropical Atlantic. In the presence of an Atlantic SST gradient, all models respond with a reduced monsoon flow (not shown)—therefore capturing at a minimum that part of the drying signal that is forced locally.

4. Discussion

[11] Several recent studies address the question of human influence on the Sahel. The GFDL GCMs reproduce the 20th century Sahel rainfall with uncanny precision, and sensitivity experiments support the anthropogenic origin of

the drought [*Held et al.*, 2005]. Conversely, [*Hoerling et al.*, 2006] report that a multi-model ensemble forced with 20th century anthropogenic emissions reproduces the long-term variations of Indian Ocean and (less accurately) Atlantic Ocean SST, but fails to reproduce the magnitude of the observed 1950–1999 Sahel drying.

[12] It is not surprising that coupled models would not faithfully and consistently reproduce the timing and magnitude of the observed trend. Even with prescribed SST, models reproduce only about 2/3 of the trend [*Hoerling et al.*, 2006], and a growing body of literature [e.g., *Sutton and Hodson*, 2005] relates internal, decadal variations in the MOC, the Atlantic gradient, and African drought. It is plausible that the abruptness and magnitude of the 1950–1999 trend were in part a consequence of internal variability in the atmosphere-ocean-land system. The forced part of the signal emerges not in a sharp 1950–1999 trend, but in the overall change in mean rainfall, a less stringent test. We claim that an internally generated, natural drying was superimposed on an externally forced, likely anthropogenic signal. A rough estimate for the role of external forcings is derived by comparing the observed 1930–1999 Sahel drying with the XX-PI difference. The former is -1.1 mm day^{-1} (25% over 70 years), the latter is, on average, -0.3 mm day^{-1} (8%), indicating that perhaps a third of the long-term drying was externally forced (or more, considering possible amplifications by vegetation and dust dynamics).

[13] The GCMs forced exclusively by anthropogenic forcings consistently reproduce the XX-PI change in global SST associated with Sahel drought and a correspondent Sahel drying, suggesting that the important external forcings are anthropogenic. Specifically, Northern Hemisphere sulfate aerosols are key for a robust drying signal in the Sahel, as they force a meridional gradient in Atlantic SST, hence reduced moisture flux by anomalous winds. In simulations where the asymmetric cooling effect of aerosols is absent or overwhelmed by the effect of increased GHG, an across-tropics uniform warming becomes the dominant signal in SST, and the precipitation response becomes model-dependent. Hence, the cross-model consensus in interpreting the history of Sahel rainfall breaks down in forecasting its future [*Held et al.*, 2005]. We hypothesize that different precipitation responses might arise from different balances between competing forcings. First, a warmer Indo-Pacific—implying a warmer, more stable free troposphere [e.g., *Chiang and Sobel*, 2002], an upped-ante for convection [*Neelin et al.*, 2003], and a drier Sahel. Second, a warmer Atlantic and increased land-ocean temperature contrast—implying stronger moisture advection by the monsoon [*Haarsma et al.*, 2005], and a wetter Sahel. Meaningful climate predictions for this vulnerable region require an understanding of what tips the balance toward a dry or wet Sahel in different models.
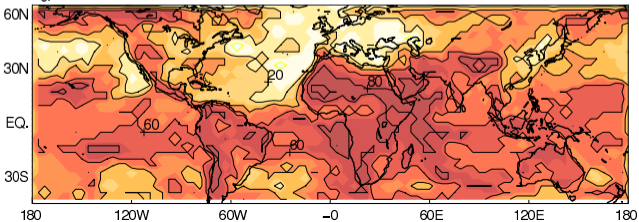
References

Chiang, J. C. H., and A. H. Sobel (2002), Tropical tropospheric temperature variations caused by ENSO and their influence on the remote tropical climate, *J. Clim.*, *15*, 2616–2631.

Cubasch, U., G. Meehl, G. Boer, R. Stouffer, M. Dix, A. Noda, C. Senior, S. Raper, and K. Yap (2001), Projection of future climate change, in *Climate Change 2001, The Science of Climate Change*, edited by J. T. Houghton, et al., pp. 527–582, Cambridge Univ. Press, New York.

Folland, C. K., T. N. Palmer, and D. Parker (1986), Sahel rainfall and worldwide sea temperature, *Nature*, *320*, 602–687.

Giannini, A., R. Saravanan, and P. Chang (2003), Oceanic forcing of Sahel rainfall on interannual to interdecadal time scale, *Science*, *302*, 1027–1030.

Haarsma, R. J., F. M. Selten, S. L. Weber, and M. Kliphuis (2005), Sahel rainfall variability and response to greenhouse warming, *Geophys. Res. Lett.*, *32*, L17702, doi:10.1029/2005GL023232.

Hansen, J., R. Ruedy, J. Glascoe, and M. Sato (1999), GISS analysis of surface temperature change, *J. Geophys. Res.*, *104*(D24), 30,997–31,022, doi:10.1029/1999JD900835.

Hansen, J., et al. (2002), Climate forcings in Goddard Institute for Space Studies SI2000 simulations, *J. Geophys. Res.*, *107*(D18), 4347, doi:10.1029/2001JD001143.

Held, I. M., T. L. Delworth, J. Lu, K. L. Findell, and T. R. Knutson (2005), Simulation of Sahel drought in the 20th and 21st centuries, Proc, *Natl. Acad. Sci. U. S. A.*, *102*, 17,891–17,896, doi:10.1073/pnas.0509057102.

Herrmann, S., and C. Hutchinson (2005), The changing contexts of the desertification debate, *J. Arid Environ.*, *63*, 538–555.

Hoerling, M., J. Hurrell, J. Eischeid, and A. Phillips (2006), Detection and attribution of 20th century northern and southern African rainfall change, *J. Clim.*, in press.

Lu, J., and T. Delworth (2005), Oceanic forcing of the late 20th century Sahel drought, *Geophys. Res. Lett.*, *32*, L22706, doi:10.1029/2005GL023316.

Neelin, J. D., C. Chou, and H. Su (2003), Tropical drought regions in global warming and El Nino teleconnections, *Geophys. Res. Lett.*, *30*(24), 2275, doi:10.1029/2003GL018625.

Nicholson, S. E. (1980), The nature of rainfall fluctuations in subtropical West Africa, *Mon. Weather Rev.*, *108*, 473–487.

Nicholson, S. E., B. Some, and B. Kone (2000), An analysis of recent rainfall conditions in West Africa, including the rainy seasons of the 1997 El Niño and the 1998 La Niña years, *J. Clim.*, *13*, 2628–2640.

Rahmstorf, S. (2002), Ocean circulation and climate during the past 120,000 years, *Nature*, *419*, 207–214.

Rotstayn, L. D., and U. Lohmann (2002), Tropical rainfall trends and the indirect aerosol effect, *J. Clim.*, *15*, 2103–2116.

Sutton, R. T., and D. L. R. Hodson (2005), Atlantic ocean forcing of North American and European summer climate, *Science*, *309*, 115–118.

Tippett, M., and A. Giannini (2006), Potentially predictable components of African summer rainfall in a SST-forced GCM simulation, *J. Clim.*, in press.

Zeng, N., J. D. Neelin, K.-M. Lau, and C. J. Tucker (1999), Enhancement of interdecadal climate variability in the Sahel by vegetation interaction, *Science*, *286*, 1537–1540.

————————————

M. Biasutti, Lamont-Doherty Earth Observatory, Columbia University, 61 Route 9W Palisades, NY 10964, USA. (biasutti@ldeo.columbia.edu)

A. Giannini, International Research Institute for Climate and Society, Columbia University, Lamont Campus, 61 Route 9W, Monell Building, Palisades, NY 10964–8000, USA.

Model	Nat	Land	OC	BC	IE
ccma_cgcm3	N	N	N	N	N
cnrm_cm3	N	N	N	N	N
csiro_mk3_0	N	N	N	N	N
gfdl_cm2_0	Y	Y	Y	Y	N
gfdl_cm2_1	Y	Y	Y	Y	N
giss_aom	N	N	N	N	N
giss_model_e_h	Y	Y	Y	Y	Y
giss_model_e_r	Y	Y	Y	Y	Y
iap_fgoals1_0_g	N	N	N	N	N
inmcm3_0	Y	N	N	N	N
ipsl_cm4	N	N	N	N	N
miroc3_2_hires	Y	Y	Y	Y	Y
miroc3_2_medres	Y	Y	Y	Y	Y
mpi_echam5	N	N	N	N	Y
mri_cgcm2_3_2a	Y	N	N	N	N
ncar_cccsm3_0	Y	N	N	Y	N
ncar_pcmi	Y	N	N	N	N
ukmo_hadcm3	N	N	N	N	Y
ukmo_hadgem1	N	N	Y	Y	Y

a. XX−PI SST in NAT+ANTHRO Models
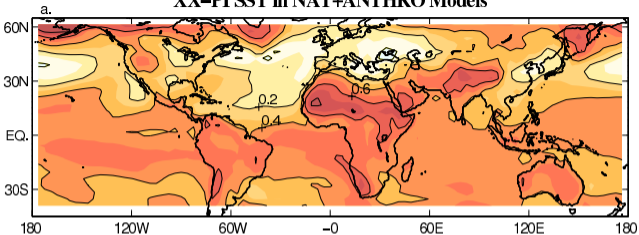
b. XX−PI SST in ANTHRO Models
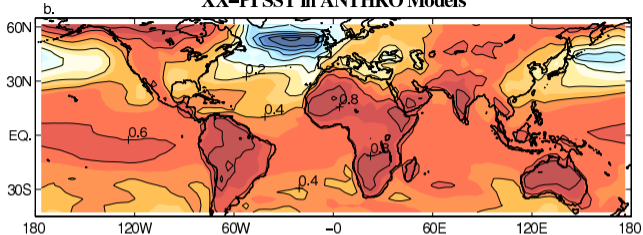
c. % of NAT+ANTHRO Models with XX−PI Mean Sfc. Temp. >.4 (<−.4)

d. % of ANTHRO Models with XX−PI Mean Sfc. Temp. >.4 (<−.4)